

The outlook of zeolite-Y hampered metal–ligand framework as heterogeneous catalysts: synthesis, spectral account and catalytic features

Jignasu P. Mehta¹ · Digvijaysinh K. Parmar¹ · Haresh D. Nakum¹ ·
Dinesh R. Godhani¹ · Nisheeth C. Desai¹

Published online: 30 May 2016
© Springer Science+Business Media New York 2016

Abstract Zeolite-Y enslaved complexes were prepared by the Flexible ligand method. Synthesized materials were characterized by various spectral tools like powder X-ray diffraction, spectral studies (UV–Vis and FT-IR), chemical analysis (ICP-OES and elemental), scanning electron microscopy, AAS and ¹H-NMR techniques. Further, BET and thermogravimetric (TG) analysis were also done for characterization of surface area, pore volume, thermal behavior, and related parameters. Baeyer–Villiger oxidation of cyclohexanone was carried out over Zeolite-Y enslaved complexes using hydrogen peroxide (H₂O₂) as an oxidant. The performance of the heterogeneous system with the homogeneous system was compared to determine the protection effect of the zeolitic matrix over the active center on the catalytic properties. In addition, the effect of experimental variables (various solvents, amount of catalyst, the mole ratio of substrate and oxidant, temperature, and reaction time) was examined in order to get absolute reaction conditions. Under the optimized reaction conditions, [Fe(nbab)₂]-Y was found to be a potential candidate, achieving 70 % ϵ -caprolactone selectivity.

Keywords Zeolite-Y · Metal–ligand framework · Heterogeneous catalyst · Cyclohexanone oxidation

1 Introduction

The Baeyer–Villiger (B–V) reaction is a significant oxidation process, providing a straight corridor to oxidize ketones to lactones or esters by organic peracids, and the lactones or esters are weighty industrial intermediates for the manufacture of polymers, pharmaceuticals, agrochemicals and herbicides [1–3]. Currently, the industrial process involves the use of m-chloroperbenzoic acid to produce ϵ -caprolactone by the oxidation of cyclohexanone [4]. However, peracids are pricey and possibly explosive, which restricts their use. Additionally, the acid by-product can reduce ester selectivity by unwanted side-reactions. Therefore, expansion of alternative oxidation methods is necessary which are commercially feasible. Conversely, catalysts are enforced for an active transfer of oxygen from the oxidant to the substrate when O₂ and aqueous H₂O₂ are used as oxidants. Aqueous H₂O₂ is a favorable oxidant for B–V reaction since the only by-product is water. Thus, the advance of catalytic B–V reaction using O₂ or aqueous H₂O₂ is essential, which satisfies the necessities of environmentally benign approaches, compared to outdated oxidation systems [5, 6].

Metal complex-catalyzed (homogeneous and heterogeneous) oxidation reactions are important reactions in chemical industry [7, 8]. The major downside of homogeneous metal complexes as catalysts is their irreversible deactivation due to the formation of μ -oxo and μ -peroxo dimeric and other polymeric species, especially when using oxidant [9]. Nanoporous materials such as framework silicates, zeolites, carbon nanotubes and nanoporous silicon have been used to iron out the kinks of homogeneous systems [10]. During the last years, there have been extreme developments in synthesis, characterization, and application of novel nanoporous materials [11, 12].

✉ Jignasu P. Mehta
jpm1569@yahoo.co.in

¹ Department of Chemistry, (UGC NON-SAP and DST-FIST Sponsored Department), Maharaja Krishnakumarsinhji Bhavnagar University, Mahatma Gandhi Campus, Bhavnagar, Gujarat 364 002, India

Especially, zeolite-Y can perform as “host materials” for incoming guest molecules due to the evenness of the pore dimensions. The stability increases by several orders of magnitude when the metal complexes are enslaved inside the nanopore of the faujasite zeolites. Enslavement of transition metal complexes inside the nanocavities of zeolite has been found to be convenient and advantageous due to the selectivity, reusability beside with thermal stability [13, 14]. Zeolite enslaved complexes is one of the subjects of the current catalysis research due to their potentiality as heterogeneous catalysts for the oxidation of alkanes, alkenes, alcohols and ketones [15–18]. Dutta et al. [19] carried out the oxidation of various cyclic ketones using Sn(salen)-NaY as a heterogeneous catalyst. They have obtained 75 % yield of ϵ -caprolactone from catalytic oxidation of cyclohexanone over Sn(salen)-NaY catalyst. Corma et al. [2] have developed tin-containing beta zeolite catalyst, which became very effective for the B–V reaction as it can catalyze the oxidation of cyclohexanone to ϵ -caprolactone with exceptional selectivity. Our laboratory has been exploring the chemistry of this class of catalysts in the last few years to improve the host–guest chemistry of zeolite-Y enslaved complexes [20–22]. In continuation of our work, in this article we report the catalytic B–V oxidation of cyclohexanone in the liquid phase over zeolite-Y enslaved complexes as heterogeneous catalysts, using H_2O_2 as an oxidant.

2 Experimental

2.1 Materials and reagents

The sodium form of zeolite-Y was purchased from Hi-media (India). 2-aminobenzoic acid, 3-nitrobenzaldehyde, 30 % hydrogen peroxide (H_2O_2) and cyclohexanone were purchased from Aldrich. Transition metal salts and solvents were purchased from Merck and used as received without further purifications.

2.2 Instrumentation

For the characterization of synthesized materials, various physico-chemical techniques have been used. ICP-OES (Model: PerkinElmer optima 2000 DV) was used to determine the composition of Si, Al, Na, Mn, Fe, Ni and Cu metal ions. The elemental analysis (C, H and N) of the materials was carried out on Perkin Elmer, USA 2400-II CHN analyzer. The surface area of materials was measured by a multipoint BET method using ASAP 2010, micromeritics surface area analyzer. XRD studies were performed on a Bruker AXS D₈ Advance X-ray powder diffractometer with a Cu-K α radiation as the incident beam

to confirm the crystallinity of compounds. The scanning electron micrographs of zeolite-Y enslaved Cu (II) complex were recorded using a SEM instrument (Model: LEO 1430 VP). The sample materials were coated with a thin gold film before taking the SEM to defend surface material from thermal damage by the electron beam. FT-IR spectra were recorded on a Thermo Nicolet IR200 FT-IR spectrometer in KBr. The electronic spectra were taken on Spectrophotometer Make/model Varian Cary 500, Shimadzu. Thermogravimetric analysis (TGA) was carried out using a thermal gravimetric analysis instrument (Shimadzu TGA-50H) with a flow rate of 20.0 mL min⁻¹ and a heating rate of 10 °C min⁻¹. Reaction products were analyzed by GC–MS has a BP-5 capillary column (30 m \times 0.25 mm \times 0.25 μ m), FID detector and 95 % silicoxane surface. The reaction products were confirmed by GC–MS model Shimadzu, QP-2012.

2.3 Synthesis of schiff base ligand

Schiff base ligand ‘nbab’ [(Z)-2-((3-nitrobenzylidene)amino)benzoic acid] was synthesized by stirring a mixture of 2-aminobenzoic acid (1.37 g, 0.01 M) with 3-nitrobenzaldehyde (1.51 g, 0.01 M) in 50 mL of ethanolic medium. The solid product formed was removed by filtration and recrystallized from ethanol.

nbab: Yellow crystals; m.p. 215–218 °C; Anal. Calcd. (%), C(62.22 %), H(3.73 %), N(10.37 %); found (%) C(62.17 %), H(3.69 %), N(10.34 %); ¹H-NMR (δ , ppm): 6.70–8.24 (8H, Ar–H), 8.60 (1H, N=CH), 10.10 (1H, –COOH); IR (KBr, cm⁻¹): –OH (str.): 3100, C=O (str.): 1692, N=C: 1635, Ar–NO₂: 1570, –OH (bend.): 1315; UV–vis (λ_{max} , nm) (transition): 216 (ILCT), 246 ($\pi \rightarrow \pi^*$), 321 ($n \rightarrow \pi^*$).

2.4 Synthesis of neat complexes

The solution of transition metal salts M(II) (where, M=Mn, Fe, Ni, Cu) of 0.01 mol in 25 mL of deionized water was added to a 25 mL of ethanolic solution of 0.02 mol ligand nbab with constant stirring. The pH of the solution was adjusted 5–6 by dropwise addition of an ethanolic solution of sodium acetate in it. The resulting mixture was heated under reflux on a water bath for 4–5 h. After cooling, the solid product was separated by filtration and dried in vacuum.

2.5 Synthesis of metal exchanged zeolite-Y

An amount of 4.0 g of zeolite-Y was suspended in 200 mL deionized water containing 12 mmol transition metal salt ($MnSO_4 \cdot H_2O/FeSO_4 \cdot 7H_2O/NiSO_4 \cdot 6H_2O/CuSO_4 \cdot 5H_2O$). The mixture was then heated with constant stirring at 100 °C for

24 h. The solid was filtered, washed with hot deionized water till the filtrate was free from any metal ion content and dried for 6 h at 150 °C in a muffle furnace.

2.6 Synthesis of zeolite-Y enslaved complexes

Zeolite-Y enslaved complexes have been prepared by flexible ligand (FL) method [23]. An amount of 1.0 g of activated metal exchanged zeolite-Y was mixed with an excessive amount of ligand nbab in 1,4-dioxane (50 mL). It was then refluxed for 12 h with constant stirring in an oil bath. The resulting solid was treated for Soxhlet extraction with acetonitrile and 1,4-dioxane to remove unreacted ligand, as well as M(II) complexes adsorbed on the external surface of the zeolite-Y. Then a material was treated with aqueous 0.01 M NaCl to remove uncoordinated metal ions. Subsequently, it was washed with deionized water to evacuate any chloride particles present, and dried at 120 °C for 12 h.

2.7 Catalytic oxidation of cyclohexanone

In order to check the catalytic performances of neat and zeolite-Y enslaved complexes, the oxidation of cyclohexanone was tested. The catalytic reaction was carried out in a two-necked 50 mL round bottomed flask. Reaction conditions for the liquid-phase oxidation of cyclohexanone were optimized as follows: cyclohexanone (1.03 mL, 0.01 mol), H₂O₂ (2.06 mL, 0.02 mol) and catalyst (30 mg) were mixed in acetonitrile (3 mL). The resulting mixture was then refluxed at 70 °C in an oil bath for 12 h with continuous stirring. After filtration and washing with a solvent, the filtrate was subjected to GC to analyze the reaction products.

3 Results and discussion

3.1 The chemical analysis data

The chemical analysis data confirmed the purity and stoichiometry of the synthesized materials (Table 1). The neat complexes derived from ligand nbab are formed by coordination with metal and ligand in 1:2 M ratio. The chemical analysis of the zeolite-Y enslaved complexes reveals the presence of organic matter with a C/N ratio almost comparable to that of neat complexes. The CHN analysis data of the neat complexes showed similarity to the theoretical values. Moreover, the Si and Al contents in the zeolite-Y enslaved complexes are almost in the same ratio as in the parent zeolite-Y. This indicates that slight variation in the zeolite framework was not due to the de-alumination during the enslavement process.

3.2 Surface area and pore volume studies

The surface area and pore volume data of zeolite-Y enslaved complexes are presented in Table 2. The enslavement of metal ions and their complexes reduce the surface area and adsorption capacity of zeolitic pores. The lowering of the surface area and pore volume supported the fact that metal complexes are present within the zeolite cages and not on the exterior surface.

3.3 Powder X-ray diffraction study

The X-ray powder diffraction (XRD) blueprint of zeolite-Y, metal exchanged zeolite-Y and zeolite-Y enslaved complexes were recorded at 2θ values between 5° and 60° to study the crystalline nature and to ensure enslavement (Fig. 1). The XRD outline of metal exchanged zeolite-Y and their respective enslaved complexes showed no momentous variations in peak positions of the diffraction lines though a slight change in the intensity of the peaks has been noticed. The relative intensities of the 311 and 220 reflections in zeolite-Y ($I_{220} > I_{311}$) were varied, i.e. $I_{311} > I_{220}$ in the case of [M(nbab)₂]-Y as well as in M(II)-Y patterns. The difference indicates the replacement of sodium ions in zeolite-Y by metal complex leads to interrupt the random distribution of small extra framework cations [24] and this variation influences the relative intensities of 3 1 1 and 2 2 0 peaks. This, of course, indicates that the enslaved complexes are responsible for the displacement of the sodium ions to locations of sodalite and center of a single six-ring (S6R) from their random positions in the super cages. These observations reveal that the enslavement of metal complex in zeolite-Y had no obvious effect on the crystallinity of the zeolitic matrix.

3.4 Scanning electron micrograph study

Scanning electron micrographs (SEMs) of [Fe(nbab)₂]-Y was taken before and after Soxhlet extraction (Fig. 2). The SEM image taken before Soxhlet extraction displays the presence of some peripheral particles on the material surface. After Soxhlet extraction, no surface complexes are seen and the particle boundaries on the exterior of zeolite are clearly distinguishable. Therefore, during the process of enslavement and Soxhlet extraction, the framework of the zeolite-Y was not damaged. These micrographs reveal the efficiency of purification method to result in complete removal of extraneous complexes, leading to the presence of well-defined enslavement in the cavity.

Table 1 The chemical composition of parent zeolite-Y, metal exchanged zeolite-Y, neat complexes and zeolite-Y enslaved complexes

Compound	C (%)	H (%)	N (%)	M (%)	C/N	Si (%)	Al (%)	Si/Al
Na-Y	–	–	–	–	–	17.16	6.60	2.60
Mn(II)-Y	–	–	–	5.74	–	16.30	6.25	2.60
Fe(II)-Y	–	–	–	6.85	–	16.62	6.39	2.60
Ni(II)-Y	–	–	–	5.98	–	16.90	6.50	2.60
Cu(II)-Y	–	–	–	6.24	–	16.13	6.21	2.60
[Mn(nbab) ₂ (H ₂ O) ₂].3H ₂ O	54.53 (55.00)	3.24 (3.30)	9.05 (9.16)	8.91 (8.99)	6.00 (6.00)	–	–	–
[Fe(nbab) ₂ (H ₂ O) ₂].2H ₂ O	54.73 (54.92)	3.19 (3.29)	9.00 (9.15)	8.97 (9.12)	6.08 (6.00)	–	–	–
[Ni(nbab) ₂ (H ₂ O) ₂].2H ₂ O	54.58 (54.67)	3.19 (3.28)	9.10 (9.11)	9.37 (9.54)	5.99 (6.00)	–	–	–
[Cu(nbab) ₂ (H ₂ O) ₂].3H ₂ O	54.16 (54.24)	3.21 (3.25)	9.00 (9.04)	10.01 (10.25)	6.01 (6.00)	–	–	–
[Mn(nbab) ₂]-Y	1.98	0.78	0.33	0.92	6.00	14.97	5.77	2.59
[Fe(nbab) ₂]-Y	2.28	0.91	0.38	0.71	6.00	15.45	5.94	2.60
[Ni(nbab) ₂]-Y	2.24	0.65	0.37	1.04	6.05	15.69	6.02	2.60
[Cu(nbab) ₂]-Y	2.32	0.83	0.39	0.88	5.94	15.81	6.08	2.60

% Found (calculated)

Table 2 Specific surface area and pore volume data

Compound	Specific surface area (m ² /g)	Specific pore volume (cm ³ /g) ^a
Na-Y	630	0.320
Mn(II)-Y	552	0.267
Fe(II)-Y	541	0.254
Ni(II)-Y	574	0.219
Cu(II)-Y	548	0.240
[Mn(nbab) ₂]-Y	345	0.174
[Fe(nbab) ₂]-Y	361	0.180
[Ni(nbab) ₂]-Y	364	0.147
[Cu(nbab) ₂]-Y	331	0.160

^a Calculated by the BJH-method

3.5 FTIR spectral study

The FTIR spectral data of ligand nbab along with neat and zeolite-Y enslaved complexes have been studied in order to characterize their structures (Table 3). As shown in Fig. 3, a sharp band is seen in zeolite-Y enslaved complexes at $\sim 1070\text{ cm}^{-1}$, which is not observed in the Schiff base ligand and their neat complexes. Hence, it could be attributed to the asymmetric stretching vibrations of (SiO₄/AlO₄) units [25]. Other major zeolite framework bands appear around 1190, 830 and 480 cm^{-1} [26]. The intensities of IR bands of the zeolite-Y enslaved complexes are weak due to the low concentration of the complex inside zeolite cavities [27].

The spectra of the neat and enslaved complexes were compared with that of the ligand nbab to determine the

coordination sites, which involved in chelation. Ligand nbab shows a strong band at $\sim 1635\text{ cm}^{-1}$ assigned to $\nu_{(\text{C}=\text{N})}$ (azomethine). While, upon complex formation, this band was shifted towards lower wave number and appears at $1605\text{--}1630\text{ cm}^{-1}$, indicates the coordination of the azomethine nitrogen to the metal ion [28]. In IR spectra of Schiff base ligand, a sharp band is observed at $\sim 1315\text{ cm}^{-1}$ attributed to aromatic -OH. Though in the case of all neat and zeolite-Y enslaved complexes, this band is completely missing, which proves the involvement of aromatic -OH in coordination with metal. The ligand shows a broad less intense band in the region $2650\text{--}2500\text{ cm}^{-1}$ point out the probability of intramolecular hydrogen bonding between O-H and azomethine nitrogen. This band disappeared completely in complexes suggests the involvement of O-H and C=N in chelation. An

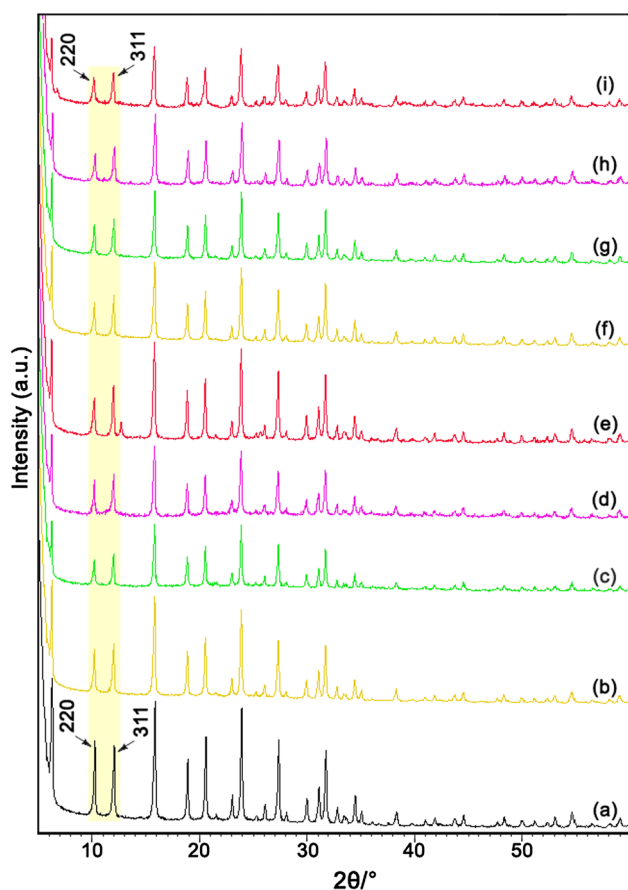


Fig. 1 XRD patterns of (a) zeolite-Y, (b) Mn(II)-Y, (c) Fe(II)-Y, (d) Ni(II)-Y, (e) Cu(II)-Y, (f) [Mn(nbab)₂]-Y, (g) [Fe(nbab)₂]-Y, (h) [Ni(nbab)₂]-Y and (i) [Cu(nbab)₂]-Y

important feature is the presence of new intense bands are observed in the far-IR region ($415\text{--}480/403\text{--}414\text{ cm}^{-1}$) in zeolite-Y enslaved complexes assigned to $\nu_{(M-O)}$ and $\nu_{(M-N)}$, stretching vibrations, which indicates the coordination of nitrogen and oxygen atoms of the Schiff base ligand to the metal ion [29]. A broadband in the region $3430\text{--}3449\text{ cm}^{-1}$, and two weaker bands in the region

$815\text{--}840$ and $670\text{--}690\text{ cm}^{-1}$ in all zeolite-Y enslaved complexes are attributed to $-\text{OH}$ stretching, rocking and wagging vibrations, respectively, of coordinated water molecules [30]. A band at 1692 cm^{-1} is assigned to $\nu_{(C=O)}$ stretching frequency in the spectrum of free Schiff base which is also shifted to a lower frequency ranging from 1654 to 1586 cm^{-1} in all the metal complexes. This indicates the involvement of oxygen atom of hydroxy group of $-\text{COOH}$ group in bonding with metal ions. Two sharp bands appeared at ~ 1320 and $\sim 1530\text{ cm}^{-1}$ shows presence stretching vibration of $-\text{NO}_2$ group in the ligand.

The zeolite-Y enslaved complexes show very analogous IR data (Fig. 3) that are shifted $2\text{--}4\text{ cm}^{-1}$ compared to those of the corresponding neat complexes (Fig. 4). Such variations may be due to distortions of the complex geometry. IR data revealed that the ligand is a bidentate uninegative ligand coordinated to the metal through one azomethine nitrogen and one deprotonated oxygen atom. Moreover, strong confirmation of the presence or absence of coordinated water was supported by thermogravimetric analysis of these complexes.

3.6 Electronic spectral study

Figure 5 show the electronic spectral data of ligand synthesized materials. The free ligand nbab exhibit three absorption bands at 246, 246, and 321 nm due to ILCT (intra ligand charge transfer transition), $\pi \rightarrow \pi^*$ (aromatic moiety) and $n \rightarrow \pi^*$ ($\text{C}=\text{N}$ chromophore) transitions, respectively. As presented in Table 4, the electronic spectrum of neat complexes showed intense bands in the range $220\text{--}310\text{ nm}$, which was assigned to $\pi \rightarrow \pi^*$ transition occur in the aromatic rings. The intense broad bands in the range $320\text{--}360\text{ nm}$ may be assigned to the $t_2(M) \rightarrow \pi^*(L)$ charge transfer transition. In addition, neat complexes shows weak bands in the range $410\text{--}725\text{ nm}$ attributed to $d\text{--}d$ transitions namely ${}^4T_{1g} \rightarrow {}^6A_{2g}$, ${}^4T_{2g}(G) \rightarrow {}^6A_{1g}$ and ${}^4T_{1g}(D) \rightarrow {}^6A_{1g}$ for Mn(II)

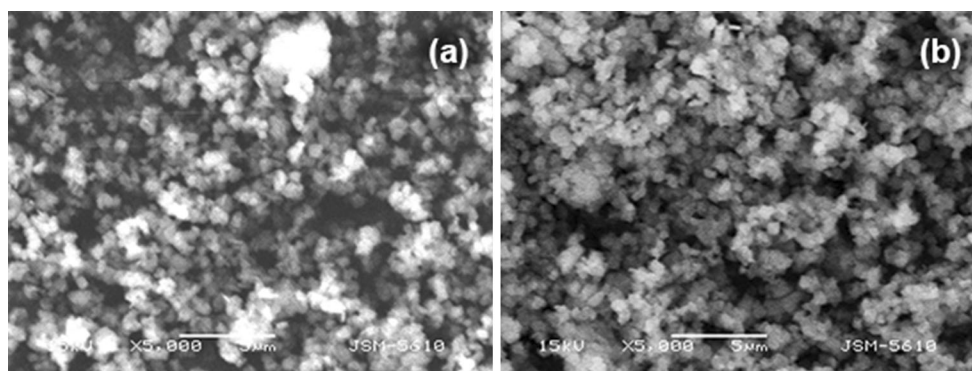
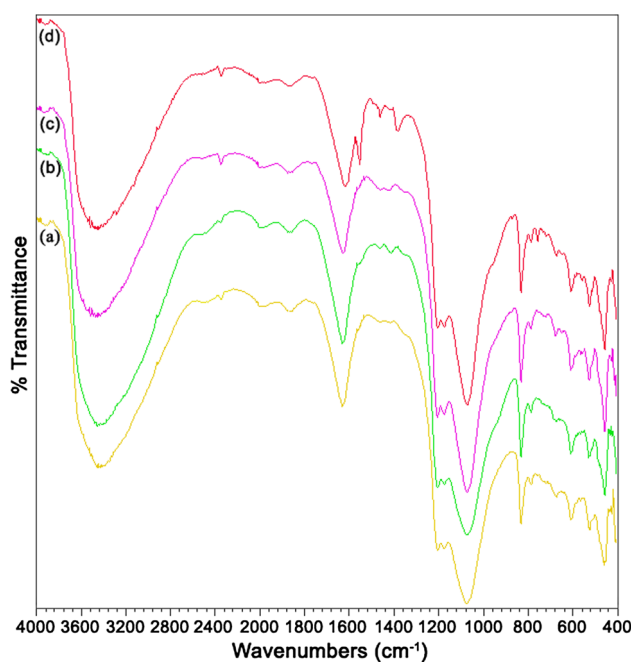


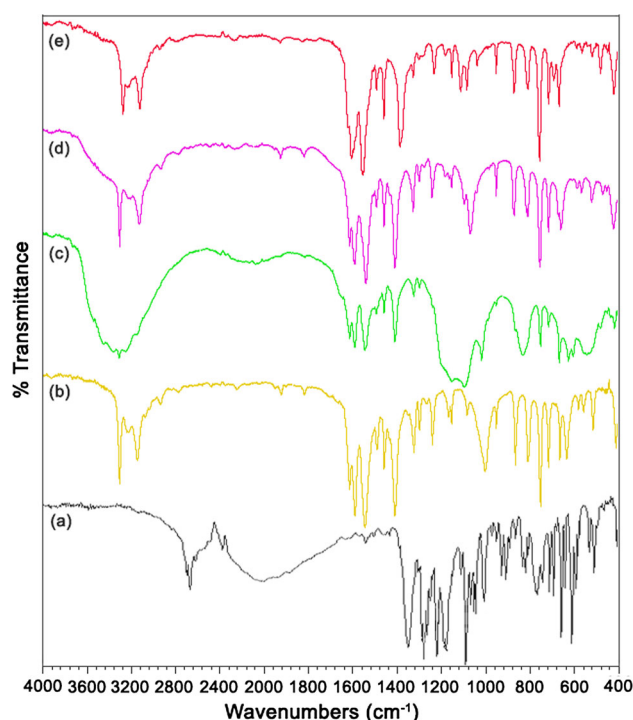
Fig. 2 SEM images of [Fe(nbab)₂]-Y a before and b after Soxhlet extraction

Table 3 FT-IR data of ligand, neat complexes, and zeolite-Y enclaved complexes

Compound	Internal vibrations			External vibrations			$\nu_{(C=N)}$	$\nu_{(O-H)}$	$\nu_{(C=O)}$
	ν_{asym} T-O	ν_{sym} T-O	ν_{bend} T-O	D-R	ν_{sym} T-O	ν_{asym} T-O			
nbab	–	–	–	–	–	–	1635	3100	1692
[Mn(nbab) ₂ (H ₂ O) ₂] \cdot 3H ₂ O	–	–	–	–	–	–	1618	3320	1590
[Fe(nbab) ₂ (H ₂ O) ₂] \cdot 2H ₂ O	–	–	–	–	–	–	1606	3324	1588
[Ni(nbab) ₂ (H ₂ O) ₂] \cdot 2H ₂ O	–	–	–	–	–	–	1614	3324	1594
[Cu(nbab) ₂ (H ₂ O) ₂] \cdot 3H ₂ O	–	–	–	–	–	–	1608	3280	1558
[Mn(nbab) ₂]-Y	1074	674	460	610	834	1178	1630	3458	1618
[Fe(nbab) ₂]-Y	1070	680	452	610	834	1176	1630	3460	1618
[Ni(nbab) ₂]-Y	1072	678	452	610	834	1178	1625	3484	1616
[Cu(nbab) ₂]-Y	1070	674	452	610	834	1176	1620	3486	1610

**Fig. 3** FTIR spectra of (a) [Mn(nbab)₂]-Y, (b) [Fe(nbab)₂]-Y, (c) [Ni(nbab)₂]-Y and (d) [Cu(nbab)₂]-Y

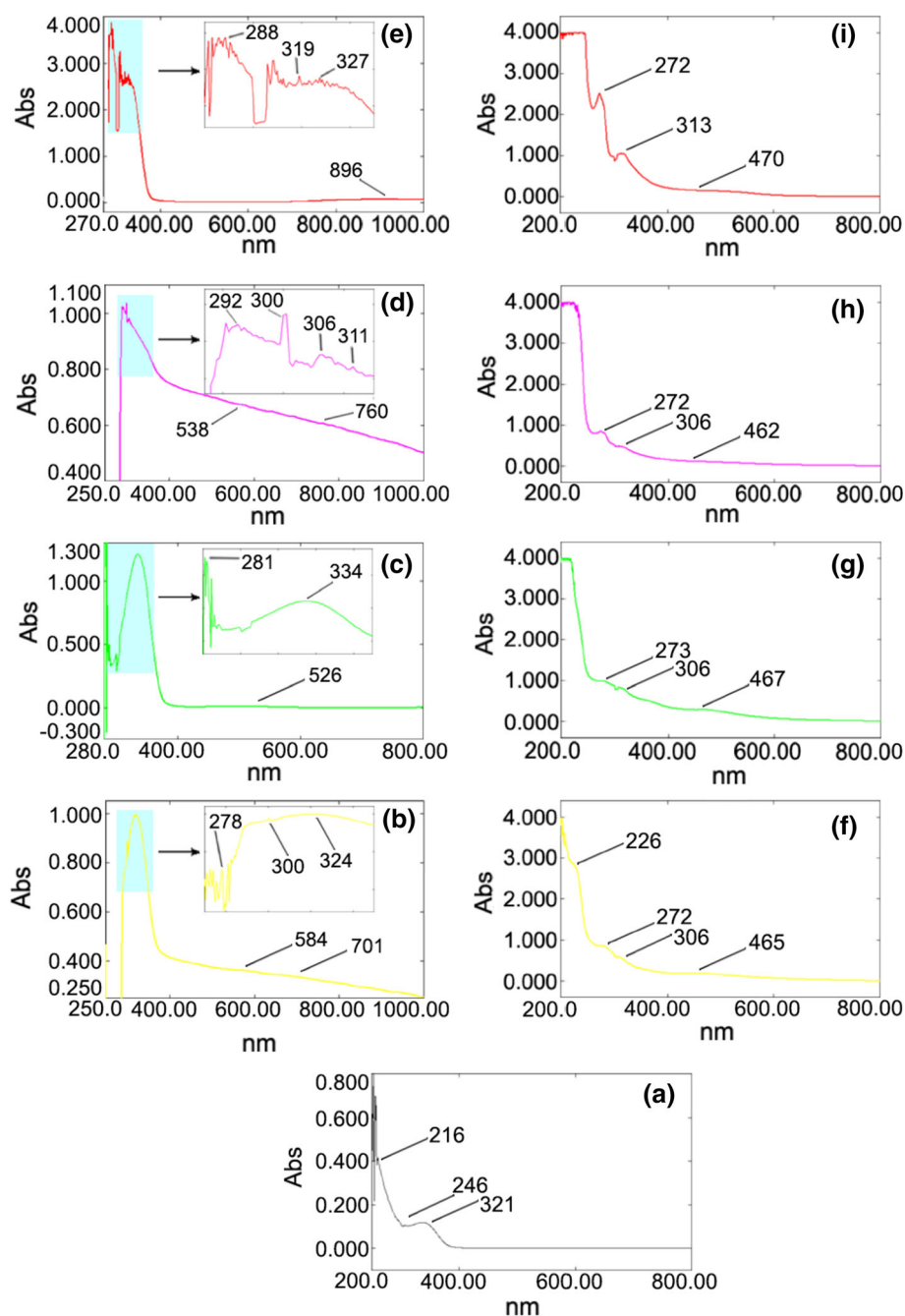
complex, ${}^6A_{1g} \rightarrow T_{2g}(G)$, and ${}^6A_{1g} \rightarrow {}^5T_{1g}$ for Fe(II) complex, and ${}^3A_{2g}(F) \rightarrow {}^3T_{1g}(P)$, ${}^3A_{2g}(F) \rightarrow {}^3T_{1g}(F)$, and ${}^3A_{2g}(F) \rightarrow {}^3T_{2g}(F)$ for Ni(II) complex, suggested an octahedral geometry for these complexes [31]. While copper complex showed the intense band at 327 nm assigned to the ligand to metal charge transfer transition and the band at 896 nm assigned to ${}^2E_g \rightarrow {}^2T_{2g}$ transition corresponding to $d-d$ transition, which justified the distorted octahedral geometry of Cu(II) complex [32]. This value is remarkably comparable to the values for the enclaved complexes. The spectra of enclaved complexes show additional absorption bands at ~ 465 nm may be attributed to $d-d$ transition. This specifies the existence of complexes inside the nanopores of zeolite-Y.

**Fig. 4** FTIR spectra of (a) nbab, (b) [Mn(nbab)₂(H₂O)₂] \cdot 3H₂O, (c) [Fe(nbab)₂(H₂O)₂] \cdot 2H₂O, (d) [Ni(nbab)₂(H₂O)₂] \cdot 2H₂O and (e) [Cu(nbab)₂(H₂O)₂] \cdot 3H₂O

3.7 Thermogravimetric (TG) analysis

The thermogravimetric analysis provides reliable evidence concerning the presence of water molecules in the coordination sphere of metal complexes. The thermal behavior of the neat and zeolite-Y enclaved complexes has been characterized by thermogravimetric (TG) method (Fig. 6). As given in Table 5, the thermal degradation of neat complexes takes place in four stages. The first stage involves the loss of hydrated water molecules in the temperature range of ~ 30 and 150 °C, followed by the loss of

Fig. 5 Electronic spectra of **a** nbab, **b** $[\text{Mn}(\text{nbab})_2(\text{H}_2\text{O})_2] \cdot 3\text{H}_2\text{O}$, **c** $[\text{Fe}(\text{nbab})_2(\text{H}_2\text{O})_2] \cdot 2\text{H}_2\text{O}$, **d** $[\text{Ni}(\text{nbab})_2(\text{H}_2\text{O})_2] \cdot 2\text{H}_2\text{O}$, **e** $[\text{Cu}(\text{nbab})_2(\text{H}_2\text{O})_2] \cdot 3\text{H}_2\text{O}$, **f** $[\text{Mn}(\text{nbab})_2] \cdot \text{Y}$, **g** $[\text{Fe}(\text{nbab})_2] \cdot \text{Y}$, **h** $[\text{Ni}(\text{nbab})_2] \cdot \text{Y}$ and **i** $[\text{Cu}(\text{nbab})_2] \cdot \text{Y}$



coordinated water molecules between ~ 151 and 300 °C. The third decomposition stage is in the temperature range of ~ 301 – 600 °C, which is attributed to the loss of ligand nbab, with the observed mass loss of ~ 70.00 %. The final residues were estimated as metal oxides. The thermal decomposition of zeolite-Y enlaved complexes usually undergoes in two stages (Table 5).

The removal of intrazeolite and coordinated water molecules takes place in ~ 30 – 200 °C temperature range. The second step starts above 450 °C, which involves the weight loss of ~ 15 % due to the decomposition of metal

complexes in this wide temperature range. This indicates the presence of only a small amount of metal complex inside the cavities of zeolite-Y.

3.8 Catalytic activity

The B–V oxidation of cyclohexanone has occurred with the formation of ϵ -caprolactone. Our work started with a sequence of scientific experiments on catalytic B–V oxidation of cyclohexanone over parent zeolite-Y, metal exchanged zeolite-Y, neat complexes, and zeolite-Y

Table 4 Electronic spectral data of ligand, neat complexes, and zeolite-Y enslaved complexes

Compound	Wavelength (nm)
nbab	216, 246, 321
[Mn(nbab) ₂ (H ₂ O) ₂] ₂ ·3H ₂ O	269, 278, 324, 584, 661, 701
[Fe(nbab) ₂ (H ₂ O) ₂] ₂ ·2H ₂ O	251, 281, 334, 526, 553
[Ni(nbab) ₂ (H ₂ O) ₂] ₂ ·2H ₂ O	292, 300, 306, 311, 538, 760
[Cu(nbab) ₂ (H ₂ O) ₂] ₂ ·3H ₂ O	269, 288, 319, 327, 896
[Mn(nbab) ₂]-Y	204, 226, 272, 306, 465
[Fe(nbab) ₂]-Y	206, 273, 306, 467
[Ni(nbab) ₂]-Y	211, 229, 272, 306, 462
[Cu(nbab) ₂]-Y	223, 236, 272, 313, 470

enslaved complexes. In a typical reaction, 1:1.5 molar ratio of the cyclohexanone (0.01 mol) and 30 % H₂O₂ (0.015 mol) were taken with 3 mL of acetonitrile, 30 mg of the catalyst was added to it and equilibrated at 70 °C in an oil-bath with constant stirring for 12 h (Table 6). The filtrate was collected at the different time and subjected to GC to identify the products.

Amongst all, [Fe(nbab)₂]-Y gives a higher conversion of cyclohexanone (Fig. 7). Therefore, [Fe(nbab)₂]-Y was taken as a representative catalyst to check the effects of solvents, catalyst amount, the mole ratio of substrate to an oxidant, and temperature with reaction time on cyclohexanone oxidation are summarized beside with their possible explanations.

The effect of organic solvents like acetonitrile, chloroform, 1, 2-dichloroethane, 1,4-dioxane, methanol, and n-butanol over catalyzed B–V oxidation of cyclohexanone have been studied (Fig. 8) by keeping other reaction parameters fixed. Among all solvents, acetonitrile shows the good activity by providing 71.03 % ϵ -caprolactone selectivity with 701 TONs. Acetonitrile is highly polar solvent, so it may readily dissolve H₂O₂ along with the cyclohexanone and consequently can direct the reactants in such a way that properly be adsorbed on the catalyst surface and thereby enhance the catalytic activity [33].

The influence of catalyst amount on the cyclohexanone oxidation was studied (Fig. 9). Five different amount of representative catalyst [Fe(nbab)₂]-Y were considered, viz., 10, 15, 20, 25 and 30 mg with the fixed amount of other reaction parameters. By varying the amount of catalyst, the conversion of cyclohexanone shows a discrepancy. An amount of 25 mg of catalyst shows a 26.4 conversion of cyclohexanone. Additionally, the TONs decreased from 846 to 701 by further raising the catalyst amount from 25 to

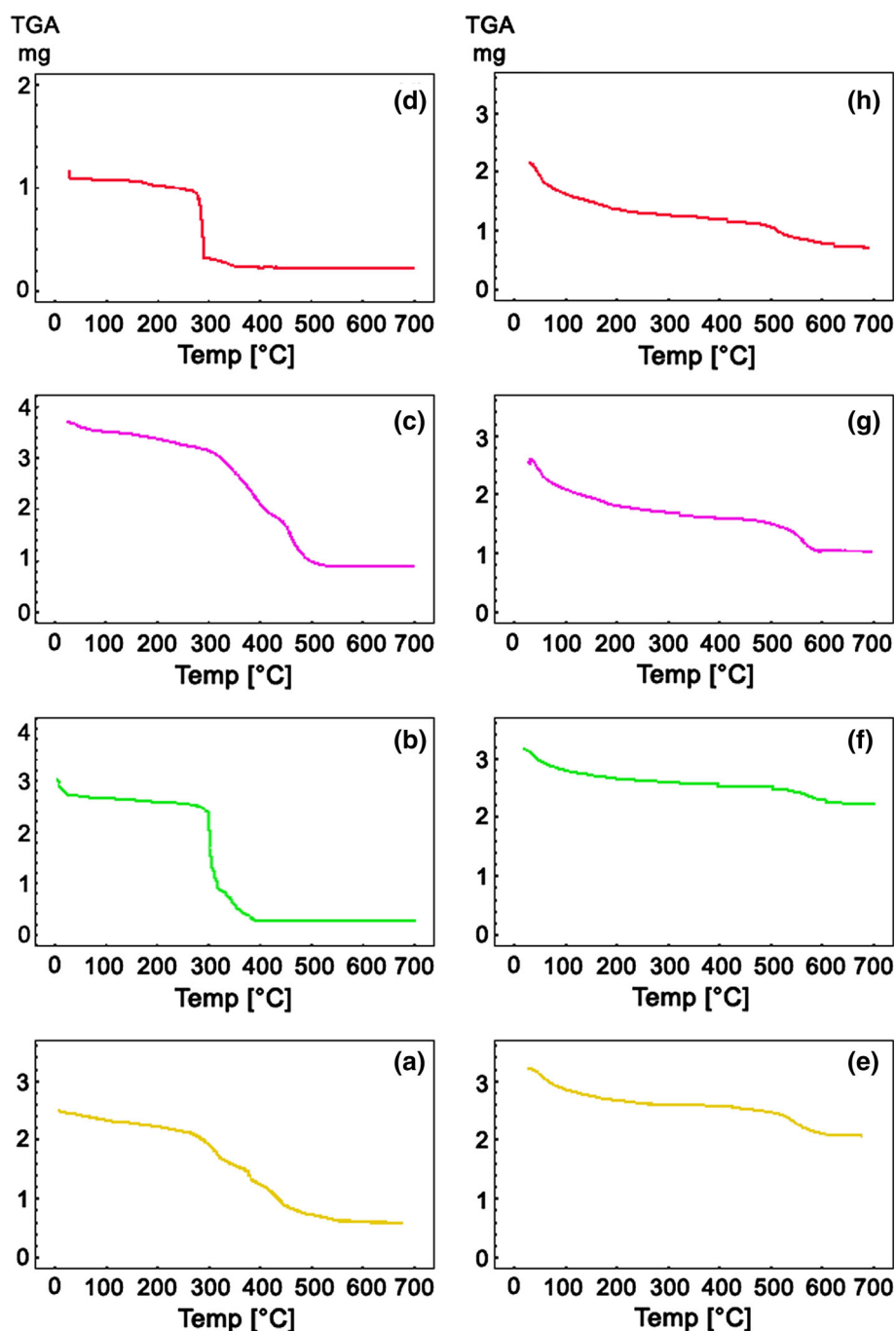
30 mg, respectively. Therefore, 25 mg amount of catalyst was taken to be optimum as there was no remarkable difference observed in the conversion when more than 25 mg of catalyst was added.

As shown in Fig. 10, four different mole ratios (1:1, 1:1.5, 1:2, 1:2.5) of cyclohexanone and 30 % H₂O₂ were taken to determine their effect on cyclohexanone oxidation by keeping all other reaction parameters fixed. Conversion of cyclohexanone was improved from 23 to 34 % upon increasing the mole ratio of cyclohexanone to 30 % H₂O₂ from 1:1 to 1:2, respectively. However, the rate of cyclohexanone conversion decreased to 31.7 % as the ratio was increased from 1:2 to 1:2.5. It may be due to a large amount of water from H₂O₂ decomposition product will dilute the reaction mixture and thus, dropping the conversion rate. The existence of excess water may have also poisoned the catalyst. Moreover, additional water also causes the further hydrolysis of ϵ -caprolactone to 6-hydroxyhexanoic acid. From the data collected, 1:2 cyclohexanone to H₂O₂ molar ratio was considered as sufficient to carry out the reaction as it gives higher TONs (1025).

The effect of temperature on the catalyst efficiency for the cyclohexanone oxidation was carried out along with different reaction time. Figure 11 shows that by increasing the temperature from 50 to 80 °C, the conversion increases from 26 to 37.3 %, respectively (for 12 h). Additionally, TONs increases from 401 to 1167, by increasing time from 3 to 12 h, respectively. Promoting higher temperature to 85 °C causes a decrease in conversion, this may be due to quick decomposition of H₂O₂. In addition, a further increase in reaction temperature and time results in low selectivity of ϵ -caprolactone viz., 74, 71, 70, 70, 68, 63, 56, and 49 % for 3, 6, 9, 12, 15, 18, 21, and 24 h reaction time, respectively (at 80 °C), conceivably due to the product over oxidation or hydrolysis [34]. Therefore, 80 °C was taken to be at the optimum temperature with a 12 h reaction time.

After optimization of reaction conditions, recycling tests of [Fe(nbab)₂]-Y were performed with a view to determining the effect of enslavement on stability (Table 7). The fresh catalyst has shown 37.3 % conversion and it is only a bit reduced to 35.7 %, even after the three consecutive runs and the selectivity of ϵ -caprolactone were not differ much as well. The recycled catalyst provides 1132, 1126, and 1126 TONs for three successive runs, respectively. Additionally, the atomic absorption spectroscopic analysis did not show any iron metal content in the filtrate, which confirms that iron is not leaching out from the catalyst during B–V oxidation reaction. The results indicate that zeolite-Y enslaved

Fig. 6 TGA data of
a $[\text{Mn}(\text{nbab})_2(\text{H}_2\text{O})_2] \cdot 3\text{H}_2\text{O}$,
b $[\text{Fe}(\text{nbab})_2(\text{H}_2\text{O})_2] \cdot 2\text{H}_2\text{O}$,
c $[\text{Ni}(\text{nbab})_2(\text{H}_2\text{O})_2] \cdot 2\text{H}_2\text{O}$
d $[\text{Cu}(\text{nbab})_2(\text{H}_2\text{O})_2] \cdot 3\text{H}_2\text{O}$
e $[\text{Mn}(\text{nbab})_2]-\text{Y}$, **f** $[\text{Fe}(\text{nbab})_2]-$
Y, **g** $[\text{Ni}(\text{nbab})_2]-\text{Y}$ and
h $[\text{Cu}(\text{nbab})_2]-\text{Y}$



complexes are almost stable to be recycled for the B–V oxidation of cyclohexanone without much loss in activity. Thus, the enslavement of complexes in zeolites is found to increase the life of the catalyst by reducing dimerization due to the site isolation and restriction of internal framework structure. Therefore, heterogenization

of metal complexes within zeolitic nanopores led to the successful preparation of efficient and selective heterogeneous catalysts for the B–V oxidation which helps to avoid suffering of metal complexes from decomposition, formation of peroxy species, and recyclability problems.

Table 5 Thermogravimetric results of neat complexes and zeolite-Y enlaved complexes

Compound	TG range (°C)	Observed mass loss (%)	Assignment
[Mn(nbab) ₂ (H ₂ O) ₂].3H ₂ O	30–150	7.15 (7.90)	Loss of three crystallization H ₂ O
	151–300	4.97 (5.27)	Loss of two coordinated H ₂ O
	301–550	76.068 (79.06)	Removal of Schiff base ligand
	551–700	11.73 (7.02)	Mn ₂ O ₃ as residue
[Fe(nbab) ₂ (H ₂ O) ₂].2H ₂ O	30–150	5.78 (5.28)	Loss of two crystallization H ₂ O
	151–300	4.99 (5.28)	Loss of two coordinated H ₂ O
	301–600	78.75 (80.65)	Removal of Schiff base ligand
	601–700	10.00 (8.4)	Fe ₂ O ₃ as residue
[Ni(nbab) ₂ (H ₂ O) ₂].2H ₂ O	30–150	5.40 (5.38)	Loss of two crystallization H ₂ O
	151–260	4.79 (5.38)	Loss of two coordinated H ₂ O
	261–550	78.21 (78.70)	Removal of Schiff base ligand
	551–700	11.58 (11.30)	NiO as residue
[Cu(nbab) ₂ (H ₂ O) ₂].3H ₂ O	30–120	7.69 (7.64)	Loss of three crystallization H ₂ O
	121–320	5.98 (5.098)	Loss of two coordinated H ₂ O
	321–510	67.53 (68.462)	Removal of Schiff base ligand
	511–700	18.80 (18.80)	CuO as residue
[Mn(nbab) ₂]-Y	50–180	8.39	Loss of intra zeolite + coordinated H ₂ O
	500–700	15.43	Decomposition of complex
[Fe(nbab) ₂]-Y	50–200	7.12	Loss of intra zeolite + coordinated H ₂ O
	500–700	16.24	Decomposition of complex
[Ni(nbab) ₂]-Y	30–180	8.74	Loss of intra zeolite + coordinated H ₂ O
	500–700	15.98	Decomposition of complex
[Cu(nbab) ₂]-Y	50–200	6.34	Loss of intra zeolite + coordinated H ₂ O
	500–700	13.41	Decomposition of complex

% Found (calculated)

Table 6 Catalytic performances of synthesized materials for the oxidation of cyclohexanone to ϵ -caprolactone with aqueous hydrogen peroxide

Compound	Conversion (%)	TON ^a	TOF (h ⁻¹) ^b	ϵ -Caprolactone selectivity (%)
Mn-Y	3.59	–	–	46.01
Fe-Y	5.66	–	–	34.85
Ni-Y	6.28	–	–	67.53
Cu-Y	6.08	–	–	23.17
[Mn(nbab) ₂ (H ₂ O) ₂].3H ₂ O	12.05	24.79	2.06	45.14
[Fe(nbab) ₂ (H ₂ O) ₂].2H ₂ O	22.29	46.34	3.86	48.35
[Ni(nbab) ₂ (H ₂ O) ₂].2H ₂ O	14.50	30.33	2.52	63.29
[Cu(nbab) ₂ (H ₂ O) ₂].3H ₂ O	19.00	40.25	3.35	31.81
[Mn(nbab) ₂]-Y	19.51	389	32	66.18
[Fe(nbab) ₂]-Y	26.71	701	58	71.03
[Ni(nbab) ₂]-Y	20.39	384	32	73.00
[Cu(nbab) ₂]-Y	20.47	493	41	28.41

Reaction conditions: 0.01 mol cyclohexanone, 0.015 mol 30 % H₂O₂, 30 mg catalyst, 3 mL acetonitrile, 70 °C, 12 h

^a TON: moles of cyclohexanone converted/mole of metal

^b TOF: moles of cyclohexanone converted/mole of metal × hour

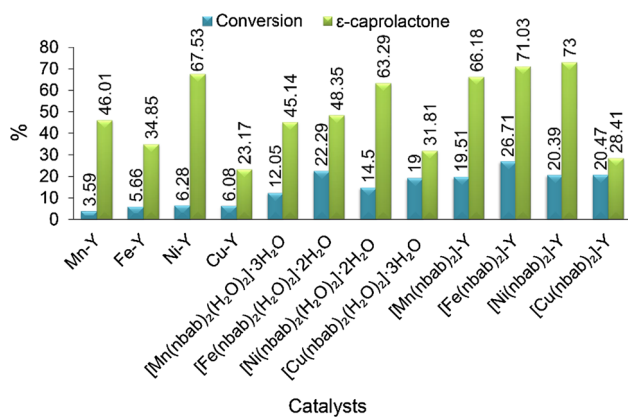


Fig. 7 Catalytic oxidation of cyclohexanone over metal exchanged zeolite-Y, neat complexes, and zeolite-Y enslaved complexes. Reaction conditions: 0.01 mole cyclohexanone, 0.015 mol 30 % H₂O₂, 30 mg [Fe(nbab)₂]-Y, 3 mL acetonitrile, 70 °C, 12 h

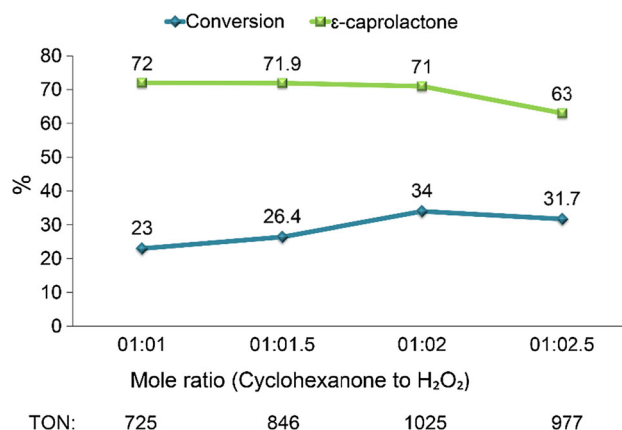


Fig. 10 Effect of mole ratio of cyclohexanone to H₂O₂ on B–V oxidation of cyclohexanone. Reaction conditions: 0.01 mol cyclohexanone, X mol 30 % H₂O₂, 25 mg [Fe(nbab)₂]-Y, 3 mL acetonitrile, 70 °C, 12 h

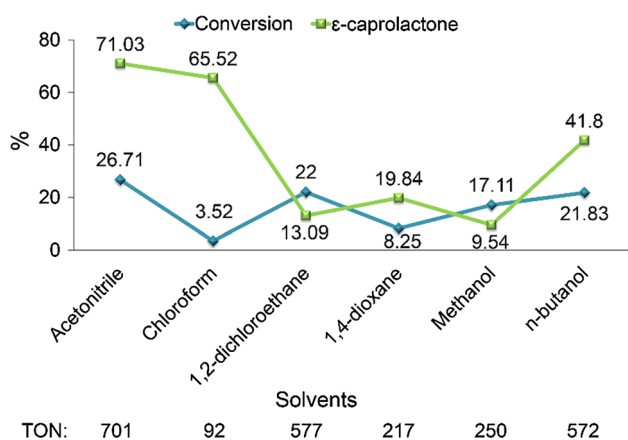


Fig. 8 Effect of solvents on B–V oxidation of cyclohexanone. Reaction conditions: 0.01 mol cyclohexanone, 0.015 mol 30 % H₂O₂, 30 mg [Fe(nbab)₂]-Y, 3 mL solvent, 70 °C, 12 h

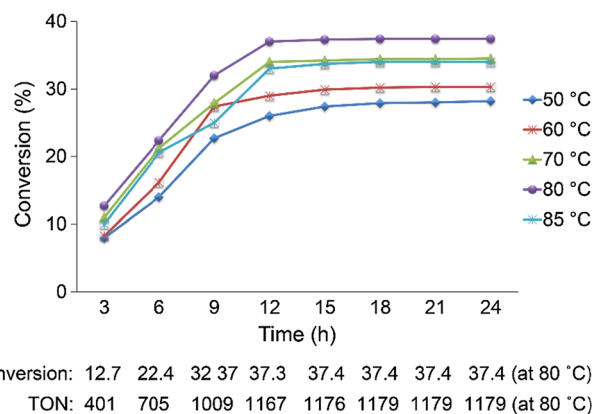


Fig. 11 Effect of temperature with reaction time on B–V oxidation of cyclohexanone. Reaction conditions: 0.01 mol cyclohexanone, 0.02 mol 30 % H₂O₂, 25 mg [Fe(nbab)₂]-Y, 3 mL acetonitrile, X °C, X h

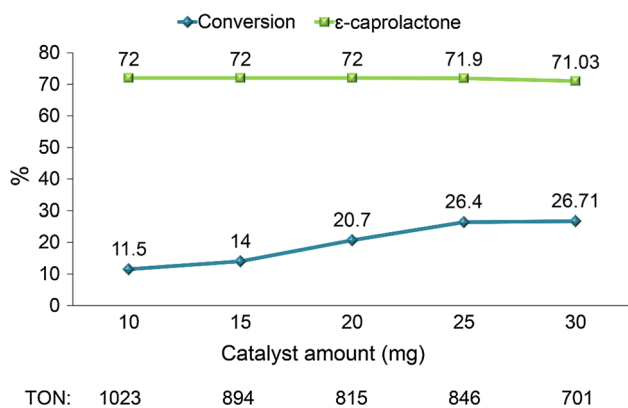


Fig. 9 Effect of catalyst amounts on B–V oxidation of cyclohexanone. Reaction conditions: 0.01 mol cyclohexanone, 0.015 mol 30 % H₂O₂, X mg [Fe(nbab)₂]-Y, 3 mL acetonitrile, 70 °C, 12 h

4 Conclusions

- In summary, synthesis of zeolite-Y enslaved complexes has been successfully done as evidenced by ICP-OES, elemental analyses, (FT-IR and UV-Vis) spectral studies, BET, SEMs, X-ray diffraction patterns, and thermal studies.
- The catalytic behaviour of synthesized materials has been tested over cyclohexanone oxidation using H₂O₂ as an oxidant.
- Factors that influence the oxidation were also meticulously checked and the optimum reaction conditions were: 0.01 mol cyclohexanone, 0.02 mol 30 % H₂O₂, 25 mg [Fe(nbab)₂]-Y, 3 mL acetonitrile, 80 °C, 12 h.
- [Fe(nbab)₂]-Y exemplifies the meaning of being heterogeneous, displayed eventual performance by

Table 7 The outcome of recovered catalyst for oxidation of cyclohexanone

Catalyst	Conversion (%)	TON ^a	TOF (h ⁻¹) ^b	ϵ -Caprolactone selectivity (%)
Fresh	37.3	1167	97.26	70.00 ^c
1st run	35.9	1132	94.37	69.87
2nd run	35.7	1126	93.83	69.87
3rd run	35.7	1126	93.83	69.85

Reaction conditions: 0.01 mol cyclohexanone, 0.02 mol 30 % H₂O₂, 25 mg [Fe(nbab)₂]-Y, 3 mL acetonitrile, 80 °C, 12 h

^a TON: moles of cyclohexanone converted/mole of metal

^b TOF: moles of cyclohexanone converted/mole of metal × hour

^c Remaining product is 6-hydroxyhexanoic acid

providing 37.3 % conversion of cyclohexanone with 70 % ϵ -caprolactone selectivity.

- Associated with their good activity, stability, ease of preparation, and appropriate performance in the recycling reaction, they appear to be environmentally benign and quite promising for specific applications.

Acknowledgments One of the authors Digvijaysinh K. Parmar is thankful to UGC, New Delhi for providing partial financial assistant (JRF) for this work.

References

- C. Bolm, *Advances in Catalytic Processes*, ed. by M.P. Doyle (JAI Press, Greenwich, 1997), pp. 43–68
- A. Corma, L.T. Nemeth, M. Renz, S. Valencia, *Nature* **412**, 423–425 (2001)
- Y.F. Li, M.Q. Guo, S.F. Yin, L. Chen, Y.B. Zhou, R.H. Qiu, C.T. Au, *Carbon* **55**, 269–275 (2013)
- H. Heaney, S.D. Burke, R.L. Danheiser (eds.), *Handbook of Reagents for Organic Synthesis: Oxidizing and Reducing Agents*, (Wiley (Chichester, UK, 1999), pp. 84–89
- T. Kawabata, Y. Ohishi, S. Itsuki, N. Fujisaki, T. Shishido, K. Takaki, Q.H. Zhang, Y. Wang, K. Takehira, *J. Mol. Catal. A: Chem.* **236**, 99–106 (2005)
- Z.H. Kang, X.F. Zhang, H.O. Liu, J.S. Qiu, K.L. Yeung, *Chem. Eng. J.* **218**, 425–432 (2013)
- R. Whyman, *Applied Organometallic Chemistry and Catalysis* (Oxford University Press, Oxford, 2001)
- M. Salavati-Niasari, *J. Mol. Catal. A: Chem.* **245**, 192–199 (2006)
- M.R. Maurya, A.K. Chandrakar, S. Chand, *J. Mol. Catal. A: Chem.* **263**, 227–237 (2007)
- F. Schuth, K.S.W. Sing, J. Weitkamp (eds.), *Handbook of Porous Solids* (Wiley-VCH, Weinheim, 2003)
- D.E. de Vos, P.P. Knops-Gerrits, D.L. Vanoppen, P.A. Jacobs, *Supramol. Chem.* **6**, 49–57 (1995)
- P.G.N. Mertens, H. Poelman, X. Ye, I.F.J. Vankelecom, P.A. Jacobs, D.E. De Vos, *Catal. Today* **122**, 352–360 (2007)
- R. Raja, P. Ratnasamy, *Catal. Lett.* **48**, 1–10 (1997)
- A. Corma, H. Garcia, *Eur. J. Inorg. Chem.* **6**, 1143–1164 (2004)
- M. Salavati-Niasari, *Inorg. Chem. Commun.* **8**, 174–177 (2005)
- B. Fan, W. Fan, R. Li, *J. Mol. Catal. A: Chem.* **201**, 137–144 (2003)
- C.R. Jacob, S.P. Varkey, P. Ratnasamy, *Appl. Catal. A: Gen.* **182**, 91–96 (1999)
- T. Kimura, A. Fukuoka, M. Ichikawa, *Catal. Lett.* **4**, 279–285 (1990)
- B. Dutta, S. Jana, S. Bhunia, H. Honda, S. Koner, *Appl. Catal. A: Gen.* **382**, 90–98 (2010)
- C.K. Modi, B.G. Gade, J.A. Chudasama, D.K. Parmar, H.D. Nakum, A.L. Patel, *Spectrochim. Acta, Part A.* **140**, 174–184 (2015)
- C.K. Modi, J.A. Chudasama, H.D. Nakum, D.K. Parmar, A.L. Patel, *J. Mol. Catal. A: Chem.* **395**, 151–161 (2014)
- C.K. Modi, P.M. Trivedi, J.A. Chudasama, H.D. Nakum, D.K. Parmar, S.K. Gupta, P.K. Jha, *Green Chem. Lett. Rev.* **7**, 278–287 (2014)
- C.K. Modi, P.M. Trivedi, *Microporous Mesoporous Materials* **155**, 227–232 (2012)
- W.H. Quayle, G. Peeters, G.L. De Roy, E.F. Vansant, J.H. Lunsford, *Inorg. Chem.* **21**, 2226–2231 (1982)
- V. Arun, N. Sridevi, P.P. Robinson, S. Manju, K.K.M. Yusuff, *J. Mol. Catal. A: Chem.* **304**, 191–198 (2009)
- B.P. Nethravathi, K.N. Mahendra, *J. Porous Mater.* **17**, 107–113 (2010)
- M.J. Alcón, A. Corma, M. Iglesias, F. Sánchez, *J. Mol. Catal. A: Chem.* **194**, 137–152 (2003)
- S. Das, S. Pal, *J. Organomet. Chem.* **691**, 2575–2583 (2006)
- K. Nakamoto, *Infrared Spectra of Inorganic and Coordination Compounds* (Wiley Interscience, New York, 1970)
- K. Nakamoto, *Infrared Spectra and Raman Spectra of Inorganic and Coordination Compounds, Part B: Application in Coordination, Organometallic, and Bioinorganic Chemistry*, 6th edn. (Wiley-Interscience, New Jersey, 2009)
- F.A. Cotton, G. Wilkinson, C.A. Murillo, M. Bochmann, *Advanced Inorganic Chemistry*, 6th edn. (Wiley, New York, 1999)
- D. Koushik, R. Jagneyeswar, M. Mario, W. Xin-Yi, G. Song, B. Pradyot, *J. Inorg. Biochem.* **101**, 95–103 (2007)
- M. Salavati-Niasari, *Inorg. Chim. Acta* **362**, 2159–2166 (2009)
- A.R. Olson, J.L. Hyde, *J. Am. Chem. Soc.* **63**, 2459–2461 (1941)